Journal of Applied Electrochemistry **34**: 781–796, 2004.

Electrocatalytic reduction of nitrate on activated rhodium electrode surfaces

PHILIP M. TUCKER[1], MICHAEL J. WAITE[1] and BRIAN E. HAYDEN[2]*
[1]*Ionex Limited, Unit 7d Nailsworth Mills Estate, Nailsworth, Glos., GL6 0BS, UK*
[2]*School of Chemistry, The University of Southampton, Southampton SO17 1BJ, UK*
*(*author for correspondence, e-mail: beh@soton.ac.uk)*

Received 1 December 2003; accepted in revised form 12 March 2004

Key words: electrocatalysis, groundwater, nitrate, reduction, rhodium

Abstract

Electrodeposited rhodium films on titanium substrates have been electrochemically activated to produce a high area surface with a specific activity for nitrate electroreduction directly to N_2. The activation process involves oxidation/reduction cycles in an alkaline, KCl electrolyte containing nitrate ions. Surfaces of up to 230 times the geometric area are achieved, together with a surface morphological modification. While the active surface, once formed, is intrinsically unstable during long-term nitrate reduction, its activity can be maintained *in situ* by an electrochemical cycling procedure. The high area rhodium has the form of a nano-structured 'sponge', with a surface area of ca. $19\,m^2\ g^{-1}$. The morphological modification is evidenced by a change in the hydrogen UPD structure, changes in the surface redox behaviour associated with OH adsorption, and a reduction in the activation energy for nitrate reduction from ca. 47 to $20\,kJ\,mol^{-1}$. The reduction in activation energy, however, is accompanied by a decrease in the pre-exponential factor, and this apparent compensation effect results in similar rate constants on the activated and unactivated surfaces. The enhancement in the catalyst's activity for nitrate reduction results from an increase in the relative activity of nitrate reduction over water reduction. The activated catalyst sustains steady state nitrate reduction at an increased over-potential before the reaction to N_2 decays, and hydrogen evolution and reduction to ammonia take place. The presence of nitrate ions is essential for the formation of the active surface, and specifically adsorbed nitrate ions and reductive intermediates are present at the surface when it is reformed. A mechanism for the elementary surface reaction steps involved in nitrate reduction, and the apparent 'habit' growth of the active surface phase in the nitrate containing solution is discussed.

1. Introduction

The nitrate ion is one of the most problematic and widespread contaminants in ground and surface waters. Natural and waste material sources of nitrate are being increasingly augmented by the impact of modern agricultural practices in both row crop and irrigated agriculture [1]. Indeed, it is the health concerns over high nitrate levels that has lead to the World Health Organisation recommending a maximum limit of $50\,mg\,l^{-1}$ in potable water [2]. Ion exchange and reverse osmosis processes have been used over the past 15 years to treat high nitrate water successfully [3]. However, both these processes merely concentrate the nitrate into an effluent stream requiring disposal. There have been increasing concerns about the environmental effects of nitrate discharges resulting in tightening legislation and increasing disposal problems and costs. A number of methods for denitrification have been investigated including biological [4], autotropic, chemical and catalytic methods. The catalytic methods can be divided into two methodologies, three phase heterogeneous catalytic and electrocatalytic. The heterogeneous catalytic reduction of nitrate in aqueous phase in the presence of hydrogen was originally based on supported palladium catalysts [5, 6], and new catalysts based on supported and promoted platinum and palladium have subsequently been investigated [7–19]. The alternative electrocatalytic method was originally explored primarily for the denitrification of solution waste materials [20–26]. Electrocatalytic denitrification has recently been applied successfully when combined with ion exchange to the denitrification of groundwater [27, 28], and has received approval for use by the UK Drinking Water Inspectorate. The subject of this paper is the basis of the latter denitrification process, which is the mechanism of the electrocatalytic reduction of nitrate on activated rhodium electrode surfaces.

The Frost diagrams for nitrogen and its compounds in acid and alkali solution [29] shows that nitrate may be reduced to N_2 in alkaline media without the formation of NO_x intermediates such as N_2O_4, which is unstable with respect to dissociation into nitrate and nitrite, and NO with respect to dissociation into nitrite and N_2O.

Thermodynamics predicts, however, that reducing all the oxides in alkaline solutions will be more difficult because the product is OH^- rather than water. This is reflected in the potential for the reaction with respect to the standard (acid) hydrogen electrode:

$$2\ NO_3^- + 6\ H_2O + 10\ e^- \rightarrow N_2 + 12\ OH^- \quad E^0 = 0.25\ V_{SHE} \tag{1}$$

$$2\ H_2O + 2\ e^- \rightarrow H_2 + 2\ OH^- \quad E^0 = -0.83\ V_{SHE} \tag{2}$$

$$O_2 + 2\ H_2O + 4\ e^- \rightarrow 4\ OH^- \quad E_0 = 0.40\ V_{SHE} \tag{3}$$

Although only a few studies have been reported for the reduction of nitrate in alkaline media the system is of interest because, in comparison to acid media, it is less likely to produce nitrogen oxide by-products and because it is less corrosive. The reduction of nitrate on the non-catalytic surface of mercury has been found possible, but only in the presence of higher-valency cations [30]. More recent work [24] has demonstrated the catalytic activity of a cobalt cyclam complex absorbed in Nafion. Reaction products included ammonia and hydroxylamine as well as nitrogen gas. There has been considerably more interest in the electrochemical reduction of nitrate on platinum group metals and metal alloys. Hobbs and coworkers [23] have reported an efficient five-electron reduction of nitrate to nitrogen on platinized nickel at 80 °C in 3 M NaOH, 0.25 M Na_2CO_3. A study by Horanyi and Rizmayer [31], also on platinized electrodes in alkali electrolyte, found that the first stage of nitrate reduction occurs at an optimum potential of around $-250\ mV_{SHE}$, whereas at more negative potentials than this the reduction appeared to be somewhat blocked by hydrogen absorption taking preference over the weak nitrate absorption required for the electron transfer reaction. It has been found [32] that the electro-reduction of nitrate in acid media is promoted more effectively on rhodium surfaces, when compared to platinum. However, most recently [33], the opposite trend in activity was suggested during studies on Rh, Pt, and alloys of the two components, in H_2SO_4 electrolyte. It was also clear from these studies that, as one may expect in acid, there were multiple pathways and intermediates formed during nitrate reduction, and the propensity of these pathways was surface and potential dependent.

We have investigated the activity of rhodium surfaces in order to optimise the conditions for nitrate reduction to N_2 over the competing processes of hydrogen adsorption and water reduction. We show that the extended rhodium surface is poisoned by hydrogen adsorption and, at potentials where higher steady state rates of nitrate reduction can be achieved, there is also a propensity for ammonia formation. In contrast, we show that a high area nano-structured rhodium surface that is able to reduce nitrate ions to N_2 at steady state without significant poisoning by adsorbed hydrogen, competitive water reduction or ammonia formation can be generated electrochemically. The rhodium catalyst can be activated and maintained by *in situ* electrochemical cycling [28]. Increases in rhodium surface areas in both acid and base supporting electrolytes have been achieved previously through fast periodic cycling to highly oxidising potentials to produce hydrous oxide layers which when reduced form high area structures [34]. The process described here achieves similar increases in surface area by cycling to lower potentials through the use of Cl^- anions to enhance the electrodissolution of the rhodium, probably through the formation of partially soluble rhodium oxychloro intermediates. However, importantly, the reduction process takes place under conditions that lead also to a morphological change, producing an active surface for nitrate reduction. We describe here the characterisation of the unactivated (low surface area starting material) and activated (high surface area and morphologically modified) rhodium catalysts in alkali-based electrolyte, and the electrochemical process leading to the restructuring of the surface.

2. Experimental

Cyclic voltammetry and steady-state measurements were carried out in a three-electrode cell assembled in a polypropylene vessel immersed in a temperature-controlled bath. Solutions were initially continuously purged with a stream of nitrogen gas to maintain the solution free of dissolved oxygen; later experiments have shown this precaution to be largely unnecessary. The potentiostat and scan generator used were built in the Electrochemistry and Surface Science Group at the University of Southampton. Experiments were carried out on rhodium wire (Johnson Matthey), rhodium-plated titanium wire or rhodium-plated titanium plate (Precious Metal Depositors UK Ltd.). The counter electrode was ruthenium-drifted oxidised titanium plate. The reference electrode was an Amagruss Sensors Refex™ electrode. This electrode employs a non-porous conductive polymer containment, which isolates the internal silver/silver chloride reference element from external contamination. Potentials are therefore given referenced to the Ag/AgCl couple. Electrolyte solutions were prepared from BDH AnalaR reagents using deionised water. Rhodium wire surfaces were cleaned initially by light abrasion (Carborundum paper) and washing with methanol. Otherwise, electrochemical surface preparation was employed as described below.

The rhodium surface areas (A_{UPD}) have been estimated using the charge associated with the hydrogen under potential deposition (UPD) measured in 0.2 M KOH in a standard scan: range −1.0 to −0.3 V, scan rate of $50\ mV\ s^{-1}$. Both the hydrogen adsorption and desorption components have been used after compensating for the underlying double layer contribution. The effective

area has been calculated assuming 8×10^{14} rhodium atoms cm^{-2} and a saturation hydrogen coverage of one monolayer. The area factor (AF) = A_{UPD}/A_G, where A_G is the geometric area of the electrode. During any electrode modification experiments, the AF was determined periodically by removing the electrode under potential control, removing excess nitrate solution (drain and rinse with deionised water), and inserting into a cell containing nitrogen saturated 0.2 M KOH solution and recording a Standard Scan from which the AF could be determined. Electrolyte samples were analysed for nitrate using an LBK Biochrom Ultrospec II UV–VIS single beam spectrophotometer.

3. Results and discussion

The activity of rhodium in sustaining steady state reduction of nitrate to nitrogen depends on its pretreatment and history within the electrolyte. A potential cycling procedure was developed to increase the surface area of the rhodium electrodes through oxidative dissolution and reduction of small concentrations of the rhodium in the region of the surface. However, after a period of cycling, during which the surface area increases substantially, morphological changes take place that affect the specific steady state activity of reduction at the rhodium surface.

3.1. *The activation of rhodium for nitrate reduction*

Generating and maintaining an active catalyst surface requires the following key conditions:

1. The electrode must be cycled between potential limits of 0.1 to −1.025 V at a cycling rate of >100 mV s^{-1}. The optimum temperature is 333 ± 5K. At temperatures in excess of 358 K the electrode tends to deactivate. The effective pH range is ca. 12.5 (between 0.2 and 0.5 M KOH). At a potential limit more positive than 0.10 V, the surface is deactivated at 333 K through the irreversible oxidation of the rhodium surface. We conclude that there are a series of competing redox reactions involving the rhodium metal mobility which have different activation energies. It is also found that cycling to potentials more negative than −1.05 V is ineffective in generating a high area active surface.
2. There must be a nitrate concentration greater than ca. 0.2 M during the initial activation process, and higher pH also assists activation (0.5 M KOH). In the absence of nitrate, cycling does not increase the surface area, and does not create a morphology change and high activity. Cycling to potentials of >−0.85 V, i.e. just over the maximum in surface reduction (see below) in the presence of nitrate, does not result in activation.
3. Chloride anions are required (>1.5 M). In the absence of Cl^-, no surface area increase and no morphology changes occur.

Figure 1 shows the voltammetry of a rhodium electrode before (1A, 1B, 1C) and after (2A, 2B, 2C) it has been subjected to activation through potential cycling. For each electrode, voltammograms are shown for the base electrolyte solution containing 0.2 M KOH and 2 M KCl, both with (A and B, solid line) and without (C, broken line) 0.3 M nitrate. The presence of KCl is required both to activate and to maintain the activity of the catalyst electrodes during steady state nitrate reduction. The currents are normalised to give current density per activated square centimetre of the catalytic electrode, and hence indicate the specific activity of the surface. In the presence of nitrate ions, the additional current associated with nitrate reduction is evident below −0.7 V. A maximum in the reductive current is

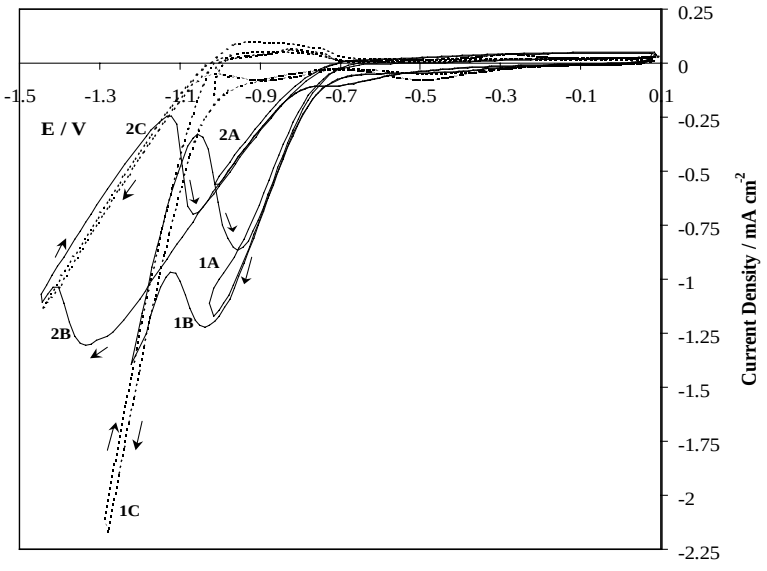

Fig. 1. Voltammetry of rhodium electrode before (1A, 1B, 1C) and after (2A, 2B, 2C) activation through potential cycling. Voltammograms for the base solution (0.2 M KOH/2 M KCl) are shown both with (solid line) and without (broken line) 0.3 M KNO_3.

evident in the extended second scans for both the activated (2B, maximum at −1.35 V) and unactivated (1B, maximum at −1.05 V) electrodes, and is a result of the competitive and poisoning reaction of water reduction at low potentials. In the case of the activated electrode, hydrogen evolution is suppressed (2C) resulting in the larger range of overpotentials in which nitrate reduction takes place. The greater activity in water reduction on the unactivated surface (1C) results in competitive poisoning at lower overpotential (1B). The result of the poisoning reaction is a strong hysteresis in the forward and reverse scans, with a recovery of the nitrate reduction on the reverse scan only when water reduction no longer competes. The same poisoning effect is observed in the results for the first scans (1A and 2A) to −1.0 V, but for the activated electrode, the rate of nitrate reduction is the same on both positive and negative going scans. For the unactivated electrode, the poisoning reaction results in a lower rate in the reverse scan.

In the absence of nitrate the surfaces show the expected hydrogen UPD structure between −0.7 and −1.0 V and the onset of hydrogen evolution at potentials below −1.0 V. However, there are differences in the hydrogen adsorption/desorption UPD structure for the two surfaces which is also evident for voltammetry in KOH (KCl free) electrolyte (Figure 4). There are also differences between the activated and unactivated surfaces in the more anodic region associated with OH adsorption and surface oxidation.

Figure 2A shows the same experimental data as that shown in Figure 1 (1A and 1C) with the current density scale expanded to show the adsorption/desorption structure more clearly for a relatively unactivated electrode. This electrode had been cycled only a few times in the electrolyte, and the data collected before significant activation had taken place, with AF = 30.

Figure 2 emphasizes the redox processes taking place in the potential range above −0.7 V. The broken curve (2) corresponds to the voltammetry in 0.2 M KOH/2 M KCl, and the solid line (1) corresponds to voltammetry in the same electrolyte containing 0.3 M KNO_3. The hydrogen UPD structure observed in the absence of the nitrate (but in the presence of Cl^-) is slightly broader than that observed in acid electrolyte on polycrystalline rhodium [35] or rhodized electrodes [36]. The redox pair (Figure 2, dotted arrow) is associated with the adsorption/desorption of hydroxide, and an additional oxidative contribution above −0.2 V can be ascribed to the onset of further surface oxidation [35, 37].

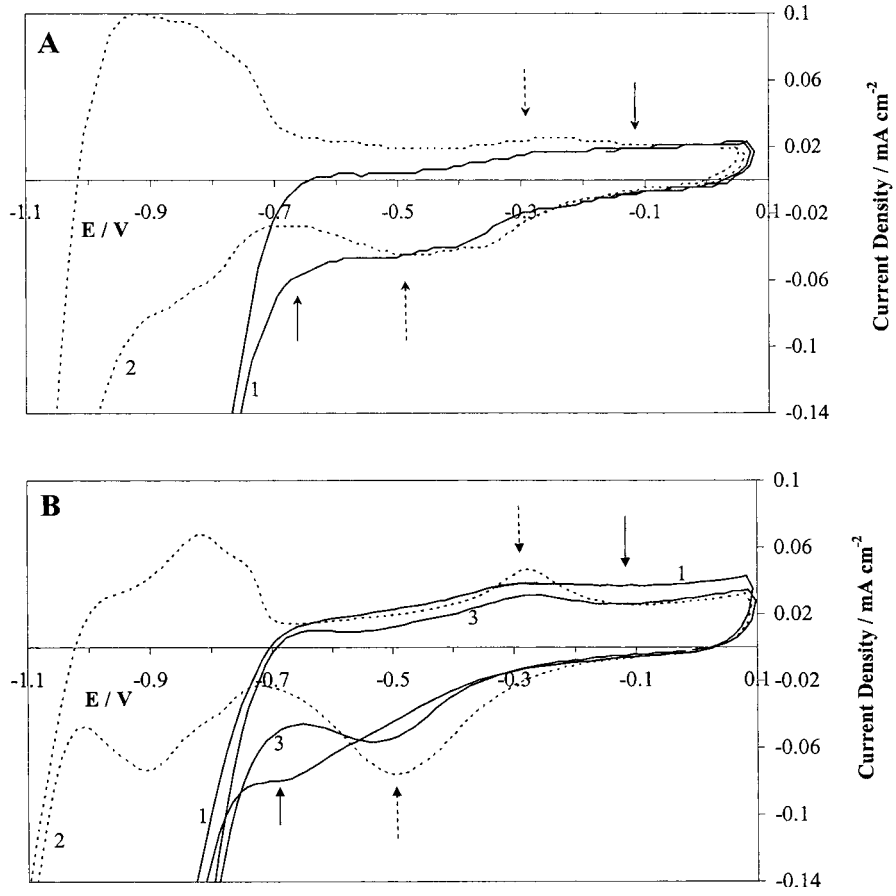

Fig. 2. Voltammetry of rhodium electrode with expanded current density scale to show hydrogen UPD and surface redox processes before (A) and after (B) activation. Figures show voltammograms for the base solution (0.2 M KOH/2 M KCl) with (solid line) and without (broken line) 0.3 M KNO_3. B (3) shows voltammogram immediately after 0.3 M nitrate addition. B (1) shows equilibrium voltammogram after development of the steady state surface structure.

The introduction of the nitrate produces a large nitrate reduction current with an onset at ca. −0.65 V. The main effect of nitrate on the surface oxidation processes is to inhibit OH adsorption and desorption, a result associated with the influence of specifically adsorbed nitrate. This effect is much more pronounced on the reconstructed surface of developed electrodes. Similar effects have been observed for a range of other anions [35, 37]. Superimposed is the underlying oxidation and reduction of the surface (solid arrows). The only effect (not shown) of the KCl that can be observed is a small shift in the OH adsorption/desorption peaks, and a very slight increase in the oxidation current in the region of potential indicated by the solid arrow. In all other aspects the presence of the Cl^- ion has no significant influence on the observed voltammetric behaviour in the anodic region. However, in the absence of the Cl^- anion, the activation (restructuring) and concomitant surface area increase does not take place. The fact that the presence of the Cl^- ion does not otherwise influence the reduction of the nitrate appears to differ from observations made in acidic conditions on rhodized electrodes where nitrate reduction is poisoned by the presence of Cl^- anions in H_2SO_4 supporting electrolyte [36].

Figure 2B shows results for voltammetry carried out under the same conditions as described for Figure 2A for an activated electrode. For the case of results obtained in nitrate containing solution, a voltammogram immediately after 0.3 M nitrate addition is shown (3), and a voltammogram obtained after cycling in the solution at 500 mV s^{-1} for 25 h to develop the steady state surface structure (1). In the absence of nitrate anions (2), the hydrogen UPD structure (−1.0 to −0.7 V) of the activated electrode is clearly changed from that of the unactivated electrode. Similar differences are observed in the voltammetry carried out in KCl free 0.2 M KOH electrolyte while recording hydrogen UPD Standard Scans (Figure 4), and are indicative of a morphological change in the rhodium surface. Specific evidence that a surface structural change has taken place on activating the rhodium is the development of the more distinctive surface redox couple, which is associated with OH adsorption/desorption (Figure 2 dotted arrow). This couple is not significantly influenced by the presence of Cl^- anions, which only shifts the peak potentials slightly. As in the case of the unactivated surface, there is an underlying surface oxidation, taking place at potentials above −0.2 V, and this appears to be enhanced on a surface which is being activated, being slightly less pronounced on a fully activated rhodium electrode surface.

The main effect of nitrate anions, in addition to inducing the expected nitrate reduction current which has its onset at ca. −0.65 V, is to suppress hydroxide adsorption and to enhance oxidation in the range −0.2 to +0.1 V (Figure 2B(1)). This oxidation is accompanied by the development of a small peak in the associated surface reduction process at the onset of the nitrate reduction region at about −0.7 V (solid arrows). It is clear therefore that there are two components in the surface reduction process and that the reduction of the surface at −0.7 V now takes place coincidentally with the onset of nitrate reduction. The effect of the Cl^- ions is to increase slightly the currents associated with this surface oxidation and reduction.

The small surface reduction component at −0.7 V (solid arrow) is sensitive to factors that impinge on the reacting surface, for example, an increase in nitrate concentration, or holding the electrode at constant potential during steady state nitrate reduction. The potential of this peak is thus clearly related to surface morphology modifications induced by the nitrate reduction which result in activation of the surface. Indeed the redox couples (Figure 2, arrows) are useful monitors of the electrode activation or deactivation. During deactivation by nitrate reduction at low nitrate concentrations (below 6000 ppm), the peak at −0.7 V decreases progressively relative to the underlying hydroxide reduction peak at ca. −0.52 V on the activated surface as the nitrate concentration reduces, and is completely removed by cycling the electrode for only several seconds in nitrate-free KOH/KCl electrolyte. It should be noted that the mid-region of the broad surface oxidation component (at about −0.1 V) appears to be associated particularly with the reconstruction processes which build up the surface area and thus its relative intensity grows as the nitrate concentration is increased and vice versa. The development of the reduction peak at −0.7 V in the presence of nitrate (a process which requires many hours of cycling) tends to mask the underlying residual hydroxide reduction peak that is shifted immediately to about −0.52 V in the presence of nitrate.

These effects are exemplified in Figure 3, which shows the voltammetry of the activated rhodium electrode, emphasising the effect of changing nitrate concentration on the surface redox couple. Results are shown for the equilibrium surface structure cycled in 8000 ppm NO_3^- (1), the electrode subsequently immersed in a base solution of 0.2 M KOH/2 M KCl (2), immediately after addition of 19 600 ppm NO_3^- (3), and, finally, after 24 h electrochemical cycling (4). The established small reductive peak at −0.7 V (formed after long periods of cycling in nitrate-containing electrolyte in (1)) is completely removed (3) by brief cycling the electrode in nitrate-free KOH/KCl (2) and it requires many hours of activation cycling through the range −1.025 to +0.1 V to restore this feature (4). These changes are accompanied by small variations in the shape of the hydrogen UPD absorption in the standard scans but the gross AF remains fairly constant. These observations appear to confirm the labile nature of the activated electrode surface morphology. The dramatic way in which the surface reduction feature is removed in the absence of nitrate (Figure 3) may reflect the sensitivity of the activated surface atomic layer to hydrogen UPD adsorption (with possible concomitant reconstruction) when nitrate ions or their reductive intermediates are not present to block specific

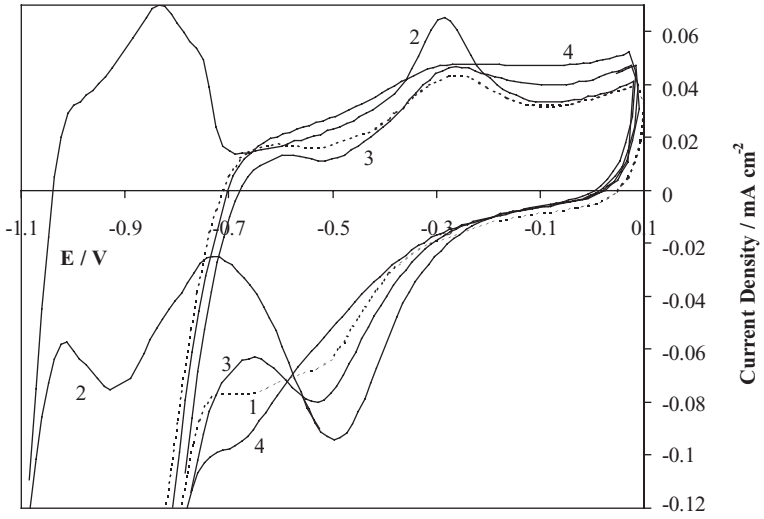

Fig. 3. Voltammetry of the activated rhodium electrode showing the effect of changing nitrate concentration on the surface redox couple, showing: (1) equilibrium in 8000 ppm NO_3^- prior to exposure to new base KOH/KCl solution; (2) scan in new base solution 0.2 M KOH/2 M KCl; (3) immediately after addition of 19 600 ppm NO_3^- ; (4) after 24 h electrochemical cycling.

surface sites. The slower rate of the redevelopment of the peak at −0.7 V (several hours electrochemical cycling) may also reflect the relative instability of the nitrate induced surface structure.

These changes in the voltammetry are attributable to significant variations in the surface morphology that are nitrate concentration dependent. These changes are also reflected in the hydrogen standard voltammetric scans used to characterise the unactivated and activated surfaces in KCl free electrolyte, examples of which are shown in Figure 4, which also shows the progressive development of an electrode. Electrodes are emmersed from the $KOH/KCl/KNO_3$ solution under potential control (−0.4 V), and after removing excess electrolyte are transferred to a 0.2 M KOH electrolyte. The standard scan was obtained at 50 mV s^{-1} (five cycles −1.0 to −0.3 V) with equilibrium being achieved after one full cycle. Both the increase in surface area (gross electrode current) and the changes that occur in the relative concentration of different surface sites (current per unit active area) during the activation process are depicted. These relative changes in surface site concentration also result in modified thermodynamic properties. Before electrode activation, the hydrogen UPD structure is similar to that found on the extended polycrystalline rhodium metal surface [35, 37] measured in acid or alkali electrolyte. The hydrogen adsorption/desorption structure on the activated electrode appears less reversible, being characterised by an apparently more strongly adsorbed species desorbing at −0.6 V in the anodic scan, and suppressed desorption of the more weakly bound hydrogen compared to the unactivated surface. These modifications induced by cycling are different to those associated with electrochemical faceting and preferred crystallographic orientation following repetitive periodic cycling in H_2SO_4 which leads to quite different hydrogen UPD characteristics [38]. The irreversibility in the UPD behaviour, however, results in an effectively hindered adsorption process (at more negative potentials on the activated surface). This behaviour is not a result of mass transport, and therefore the apparent small overpotentials in adsorption and desorption may be a result of e.g. hydrogen induced surface reconstruction. An alternative possibility is the influence of adsorbed OH on the activated surface, since this species is desorbing at more negative potentials on this surface (Figure 3). In addition to the differences in the hydroxide absorption/desorption and the hydrogen UPD behaviour, an additional difference between the activated and unactivated electrodes is their relative ability to evolve hydrogen (Figure 1). Water reduction on the unactivated electrode takes place at a significantly higher rate than on the activated electrode. This difference is also ascribed to structural modification of the rhodium surface during catalyst activation.

The change in AF as a function of time during the activation of a rhodium electrode is shown in Figure 5A. The electrode activation was carried out by cycling between potential limits of 0.1 to −1.025 V at 500 mV s^{-1}. The electrolyte was 2 M KCl/0.2 M KOH, with a nominal nitrate concentration of 0.3 M. The concentration of nitrate ions during electrode activation is also shown in Figure 5A. The activation process results in nitrate reduction, and the concomitant decrease in nitrate concentration with time is intermittently compensated by addition of nitrate ions to the solution. For this electrode, there was an initial strong increase in AF with time up to ca. 500 h, followed by a steady decrease to a limiting value of AF = ca. 160. There appears to be a surface rearrangement taking place relatively early on during activation, leading to an increase in surface area, and a second (slower) process which tends to lead to a slight decrease in surface area. Electrochemical cycling in low nitrate

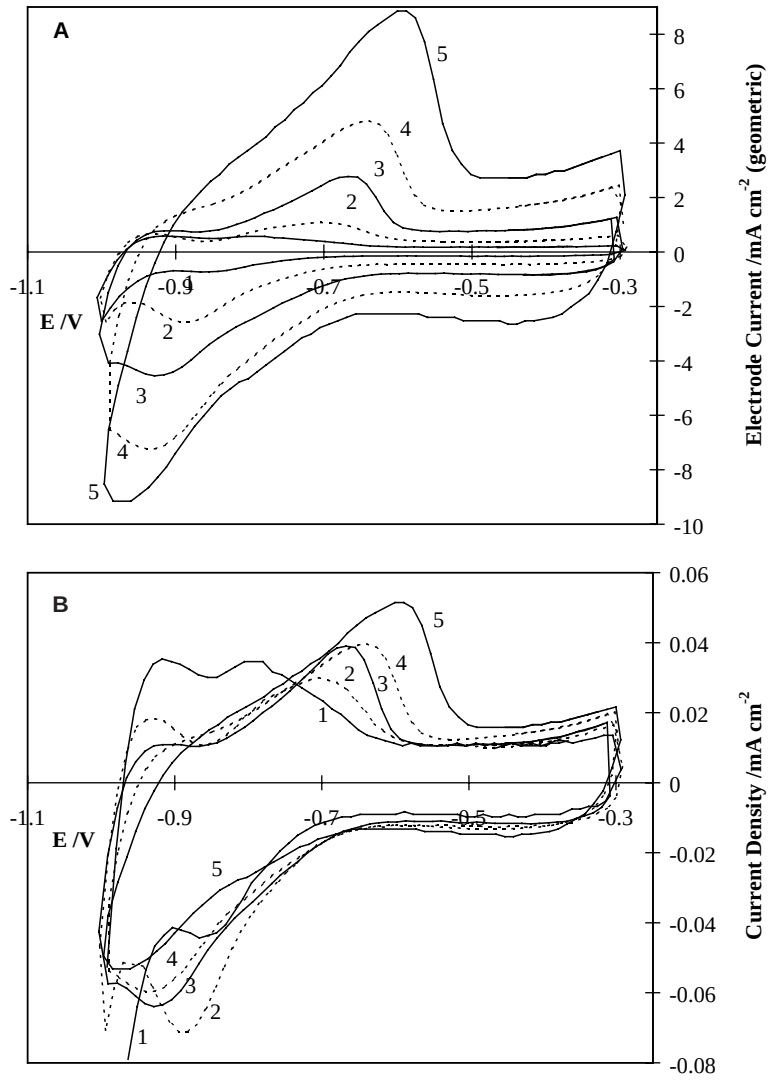

Fig. 4. Standard hydrogen voltammograms in 0.2 M KOH showing development of an electrode during its activation by electrochemical cycling (EC). Figures show (A) total electrode current and (B) specific current density. (1) 0.5 h, AF=17, ΔE_a=35 kJ mol^{-1}; (2) 69 h, AF=36, ΔE_a=44 kJ mol^{-1}; (3) 167 h, AF=66, ΔE_a=39.5 kJ mol^{-1}; (4) 831 h, AF=121, ΔE_a=27.9 kJ mol^{-1}; (5) 2025 h, AF=171, ΔE_a=22.3 kJ mol^{-1}.

concentrations <6000 ppm (0.1 M) tends to reduce AF after the initial high area structure resolves to the equilibrium level.

Figure 5B is a plot of the activation energy (ΔE_a) for nitrate reduction on the electrode surface measured at intervals during the generation of the active electrode. The details of the measurement of ΔE_a will be given below. Although there is a variation in the value of the activation energy depending upon the precise state of the electrode at any instant, there is a clear trend in the data over time. A decrease in ΔE_a is observed to take place over the first 2500 h. In addition to a gross increase in the surface area, a net morphological change takes place during activation, and the latter is associated primarily with the slower of the two processes which also seems to involve the formation of the non-reversible peak at −0.6 V in the hydrogen standard scans discussed below. As might be expected, the value of the activation energy is susceptible to the state of the surface.

Figure 4 shows the change in the intensity and relative shape of the hydrogen UPD structure in the standard scan data acquired during electrode activation. There is a progressive shift in the peak position in the oxidative sweep. There is a clear increase of a component at −0.6 V during the latter stages of the activation. This trend is seen in Figure 6 which presents the change in the UPD peak height components as a function of ΔE_a. The peak component heights at −0.6, −0.7, −0.8 and −0.9 V (normalised to the double layer charge which is proportional to area) are plotted as a function of ΔE_a. There is a correlation between the development of the hydrogen UPD peak at −0.6 V and a lowering of ΔE_a for nitrate reduction (Figure 6). The data (Figures 4–6) shows that the development of this peak requires from 500 to 1000 h. An important feature of the activated surface phase is its relative stability over changes in nitrate concentration; Figure 5 shows that AF remains reasonably constant, varying within the band 160 ± 10 for a nitrate concentration range of 6000–20 000 ppm.

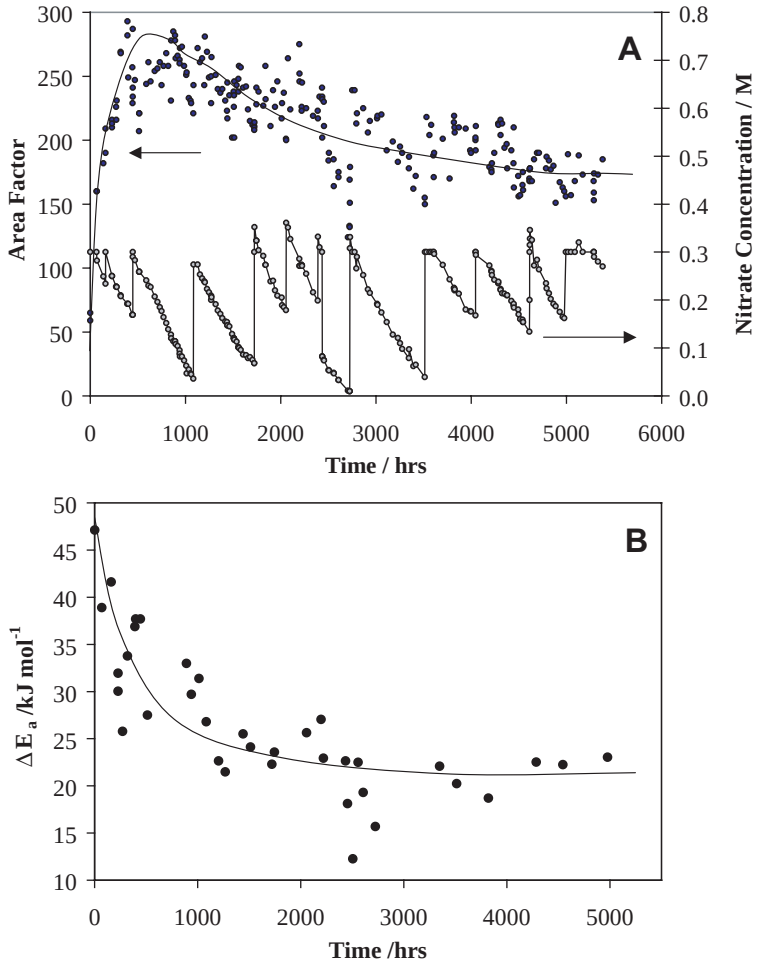

Fig. 5. AF and ΔE_a as a function of electrochemical cycling time. A shows the development of the AF of an electrode and the concomitant changes in nitrate concentration. B shows the progressive reduction in the activation energy.

It is difficult to define the precise changes in surface morphology induced by the activation process, or the detailed mechanism by which it takes place. Nevertheless, the results described above concerning the change in electrochemical behaviour induced by activation, and the conditions required to achieve it, allow some observations. The relatively mild anodic conditions used to activate the surface in the presence of chloride ions compared to the cycling conditions required to increase the surface area in the absence of chloride [34] (anodic limit of 2.0 V_{RHE}) is likely to be a result of the increased solubility of rhodium oxychlorides. It is the re-reduction of a small concentration of these solvated species near the surface that results in the formation of the high area surface in the cathodic scan. Analysis of the electrolyte after electrodes are held at ca 0.3 V indicates traces of rhodium in solution, although no rhodium is present following the cycling of the electrode potential. The formation of the high area surface specifically active in the reduction of nitrate, however, requires the presence of nitrate ions in solution. Their greatest influence in the process will be during the reduction of the oxychloride species in the reformation of the rhodium surface, since nitrate reduction is taking place during this process (Figures 2 and 3). The result is that there is a finite surface concentration of oxygen species (nitrate reduction intermediates) present on the surface during the reformation of the surface. We suggest that these adsorbed species impose crystal habit during growth. Such processes are well documented for the formation of the crystal structures of minerals [39], the effects of impurities and additives on crystal growth [40], and during the growth of compound semiconductors with preferential crystallographic planes [41, 42].

In the case of the growth of the rhodium surface we speculate that it is preferential growth of faces with sites optimal for the adsorption of the oxygen species that are generated. Evidence for this is the enhanced oxidative dissolution of the activating surface, the shift to more negative potentials of the surface reduction, and the suppression of hydrogen adsorption and irreversibility of hydrogen UPD. There is also indirect evidence from the kinetics of surface reduction on the activated surface which points to a surface structure that stabilises the reactive (oxygen bound) intermediates in nitrate reduction. The reduction in ΔE_a for the initial N—O bond breaking on the activated surface can be explained through a reduction in barrier associated with the

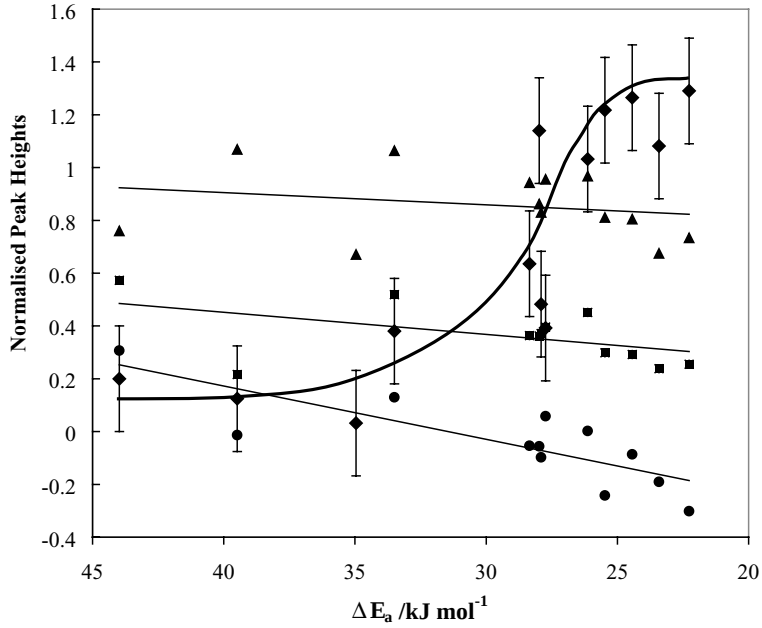

Fig. 6. Change hydrogen UPD peak height components in the anodic scan as a function of nitrate reduction activation energy ΔE_a. (1) −0.6 V (♦); (2) −0.7 V (▲); (3) −0.8 V (■); (4) −0.9 V (●).

stabilisation of the products (the Brønsted–Polanyi relationship [43]).

3.2 *Nitrate reduction on activated and unactivated rhodium*

Figure 1 showed the voltammograms for both an activated and unactivated rhodium electrode in the base electrolyte solution (0.2 M KOH and 2 M KCl) both with (solid line) and without (broken line) 0.3 M nitrate. The onset of nitrate reduction is observed at about −0.7 V. The rate of nitrate reduction on the activated and unactivated surfaces increases on the cathodic scan to a maximum before decaying and subsequently following the hydrogen evolution curve at the most negative potentials. The observed behaviour, i.e. the switching from nitrate reduction to water reduction, is a result of the competition between the two processes. The water reduction reaction hinders the nitrate reduction as a result of the blocking of the surface sites to nitrate adsorption by adsorbed hydrogen. Both hydrogen evolution and hydrogen adsorption is suppressed to more negative potentials on the activated surfaces (Figures 1 and 4). Note that on both activated and unactivated surfaces, nitrate reduction takes place at the same potential as UPD hydrogen adsorption can take place. This may not be a coincidence, and be indirect evidence that adsorbed hydrogen is involved in the removal of reductive intermediates formed via the rate determining step in nitrate reduction (N—O bond scission). However, it is evident that adsorption of hydrogen eventually leads to the poisoning of the nitrate reduction reaction, as has been surmised previously [32]. The main difference between nitrate reduction on the activated and unactivated electrodes is that the reaction is hindered by the competing water reaction only at much more negative potentials on the activated electrode. The result is that there is a much wider range of potentials on the activated electrode where steady state nitrate reduction can take place without the reaction being poisoned by adsorbed hydrogen.

We conclude that morphological modification results in this suppressed hydrogen adsorption and evolution on the activated electrode. Evidence for the morphological changes in the surface structure is found in differences in the activity to water reduction (Figure 1), changes in the hydroxide redox structure (Figures 2 and 3), changes in the hydrogen UPD structure (Figure 4), and changes in the activation energy associated with the nitrate reduction process. This difference in the activated surface to reduce nitrogen preferentially over water through a larger potential range is also reflected in the steady state measurements.

Figure 7 shows the nitrate concentration dependence of the reduction reaction as measured by cyclic voltammetry on the unactivated (Figure 7A) and activated surface (Figure 7B). The results show a similar trend for both surfaces; the effect of increasing nitrate concentration is to extend the range of potential in which nitrate reduction can take place before the competing water reduction process leads to poisoning of the nitrate reduction. The peak in the nitrate reduction current moves to more negative potentials. For the activated electrode this potential is more negative than for the unactivated electrode, at any given nitrate concentration. Figure 7C shows the concentration dependence of the reaction rate for the two surfaces, in the absence of hydrogen poisoning, using data derived along the leading edge of the reduction peak at a potential of −0.85 V. The fitted curves assume the rate of reaction is

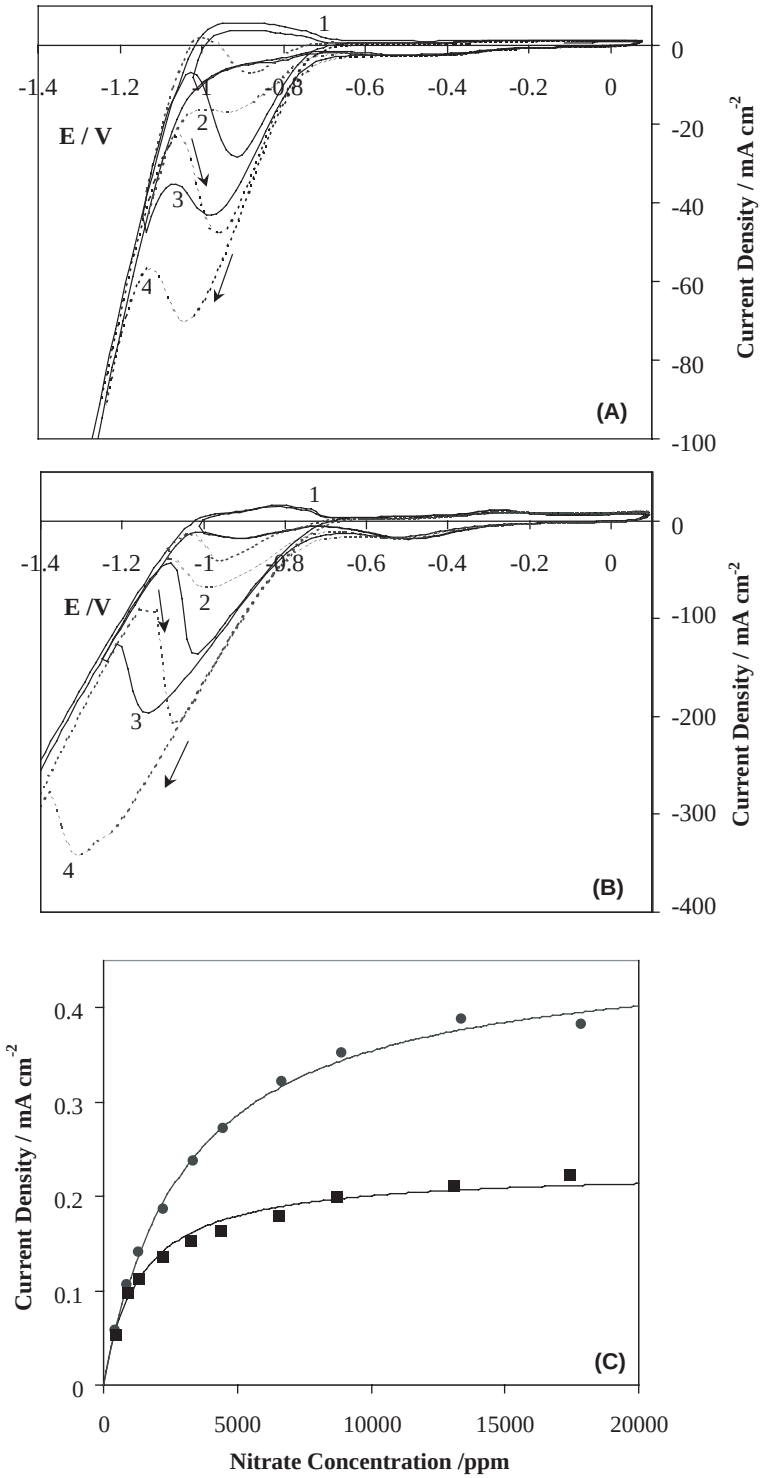

Fig. 7. The nitrate concentration dependence of nitrate reduction for (A) the unactivated surface and (B) the activated surface. (1) 0 ppm nitrate ; (2) 1472 ppm nitrate; (3) 7359 ppm nitrate; (4) 19 624 ppm nitrate. C shows the data for the reaction rate for the two surfaces at −0.85 V for the unactivated (●), and activated (■), surface.

limited by the concentration of adsorbed nitrate anions at the surface. The rate is first order in surface nitrate concentration (rate $= k\Theta_{\text{nitrate}}$), and Θ_{nitrate} is given by the Langmuir Isotherm. The rate constant k is that of the rate limiting step, N—O bond scission, and associated activation energy is obtained below. The Langmuir constant b is similar for the two surfaces ($b = 7 \times 10^{-4}$ and 3×10^{-4} for the activated and unactivated surfaces in Figure 7C) indicating that the activity of the rhodium surface has not significantly altered the specific adsorption characteristics of the nitrate anion. The difference in the absolute rate of the reaction, and hence k ($k = 2.3 \times 10^{-1}$ and 4.6×10^{-1} for the activated and4 unactivated surfaces in Figure 7C), is a result of

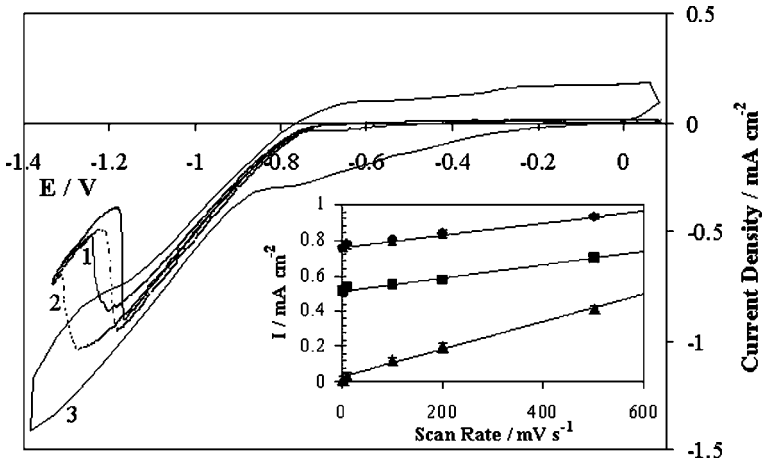

Fig. 8. Sweep rate dependence cyclic voltammetry for an activated rhodium electrode with AF=230. (1) $2\,mV\,s^{-1}$; (2) $10\,mV\,s^{-1}$; (3) $200\,mV\,s^{-1}$. Inset: current density for nitrate reduction at constant potentials of −1.1 V (●); −1.0 V (■); −0.6 V (▲).

difference in the intrinsic rate of the nitrate reactions on the two surfaces. At potentials furthest from those where hydrogen poisoning takes place, the specific rate of reduction of nitrate (turnover per rhodium atom) on the unactivated surface is in fact higher than on the activated surface.

The poisoning of the nitrate reduction by hydrogen is supported by the sweep rate dependence measurements of the cyclic voltammetry (Figure 8) measured at sweep rates between 2 and $500\,mV\,s^{-1}$. The inset in Figure 8 shows a plot of the current density for nitrate reduction measured at constant potentials of −1.1, −1.0 and −0.6 V. The electrode was an activated rhodium catalyst with AF = 230. At −0.6 V the current is dominated by the surface redox process associated with OH desorption. This is consistent with the linear scan rate dependence observed at this potential corresponding to a pseudo-capacitance of $8.2\,F\,m^{-2}$, a value near that expected (ca. $13\,F\,m^{-2}$) for the desorption of a Langmurian OH monolayer. In contrast, a smaller linear increase with a common gradient from a 'steady state' limiting (nitrate) reduction current is observed at −1.0 and −1.1 V, conditions under which nitrate reduction is taking place. The linear increase corresponds to capacitance of $3.7\,F\,m^{-2}$, significantly higher than that expected from the double layer. Its origin is likely to be residual pseudo-capacitance associated with the OH desorption which is taking place concomitantly with nitrate reduction.

The second effect of increasing the scan rate on the nitrate reduction is to increase the potential range where the nitrate reduction dominates over water reduction to more negative potentials i.e. the peak maximum moves to negative potential. This reflects the time dependence of the competing hydrogen adsorption, which must take place to poison nitrate reduction.

In order to investigate the kinetics of the reduction reaction in the region of potential where the blocking reaction was least significant, the temperature dependence of the reaction rate (as measured in the cyclic voltammetry at a potential of −0.85 V) was measured as a function of temperature in the range $355 > T/K > 295$. A typical Arrhenius plot of the reduction current measured at −0.85 V is shown in Figure 9A. Also shown is the same measurement made near the peak maximum at −1.0 V. The linear fits to the data correspond to an activation energy $\Delta E_a = 30\,kJ\,mol^{-1}$ in both cases, with pre-exponential factors of 2×10^4 and $5\times10^4\,mA\,cm^{-2}$ respectively. This data was measured on an activated catalyst with AF = 120. It is evident that the blocking reaction is not influencing the activation energy of the reduction reaction significantly in this range. The change in ΔE_a during the activation of an electrode (Figure 5B) was extracted using the above procedure. The value for the completely unactivated electrode was $\Delta E_a = 47\,kJ\,mol^{-1}$, and following activation was $\Delta E_a = 22\,kJ\,mol^{-1}$.

We associate this temperature dependence with the rate-determining step of the reduction reaction on the rhodium surface, which is likely to be the first N—O bond scission. At low concentration nitrite reduction on rhodium is much faster than nitrate reduction. The activation energy ΔE_a and pre-exponential factor A extracted from the Arrhenius plots for the rate at −0.85 V are shown in Figure 9B and C respectively. These values are shown for a variety of rhodium surfaces during the activation of different catalysts, and are characterised by the surface AF of each sample, and whether the surface is activating (●) solid line, or has been activated (■) dashed line.

Activating and activated electrodes are distinguished by diminished water reduction activity and the improved steady state nitrate reduction capacity discussed above. Activated electrodes exhibit the non-reversible hydrogen UPD structure with a well developed anodic scan peak of −0.6 V (Figures 4 and 6). All these features are the result of morphological change in the surface. A virgin rhodium electrode has an AF of ca. 15–40 (depending

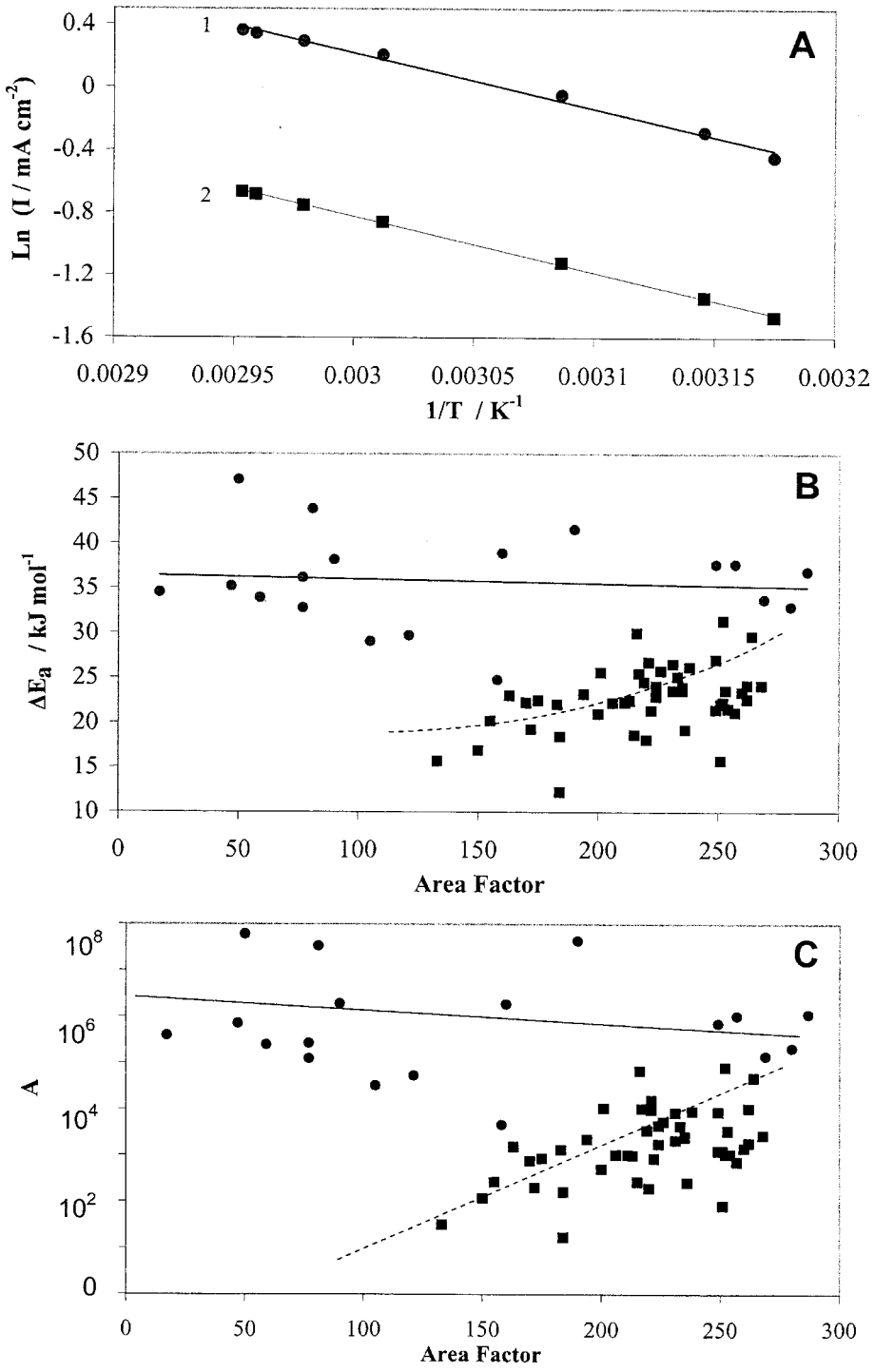

Fig. 9. The kinetics of nitrate reduction on the activating rhodium surface. A Arrhenius plots at −1.0 V (●); and −0.85 V (■). B shows change in ΔE_a, and C shows the variation in the pre-exponential factor A, for the activating (●), and activated (■) surface.

upon variations in rhodium plating), and during activation the first process to take place is an increase in AF (Figure 5A). This process generally takes place more quickly than the surface reconstruction resulting in a lowering of ΔE_a that continues while AF subsequently reduces slightly from its maximum value during cycling. The same trend is reflected in the results presented in Figure 9B and C which show that the characteristics of the activated surfaces (■) predominate once the main area increase has taken place. Once the AF reaches 150–220, the surface morphology changes and the surface AF partially decreases, and ΔE_a and the pre-exponential constant A both decrease (Figure 9B and C).

There appears to be a compensation effect in the relationship between the ΔE_a and A, and this is best exemplified in the plot (sometimes referred to a Constable plot) in Figure 10A. This is an example of a compensation effect on a series of congruent catalysts rather than between a series of related reactions [44]. The observed effect is unlikely to be associated with

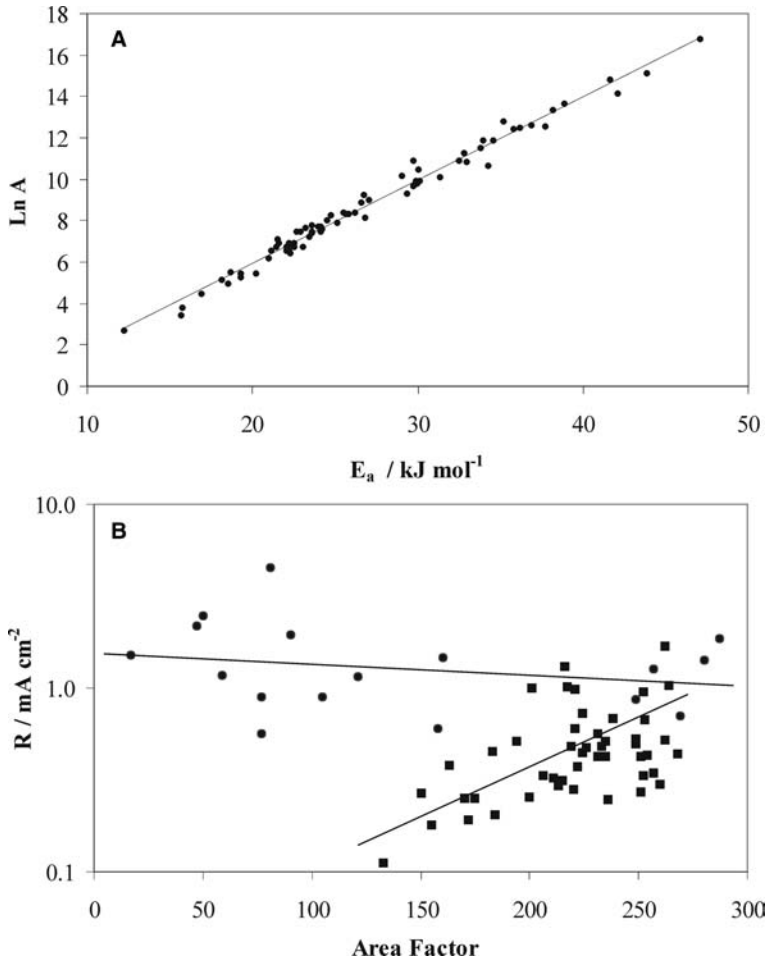

Fig. 10. The apparent compensation relationship between ΔE_a and pre-exponential constant (A), and R, specific rate constant for nitrate reduction at 333 K (B) for unactivated (●), and activated (■) electrodes.

systematic changes in effective coverage [45–47]. There is no change in the adsorption enthalpy measured on the activated and unactivated surfaces due to the fact that we are measuring an effective value of ΔE_a and A from the experimentally measured rate constant which reflects intrinsic rate constants for specific surface rhodium sites. It is the proportion of these sites that change during electrode activation. The compensation effect may reflect a common transition state, with the lower activation energy being associated with a smaller number of reaction sites on the activated surface. The net result of the changes in ΔE_a and A is that, at 333 K, the value of the specific rate constant of the nitrate reduction reaction on the activated surface is slightly lower than on the unactivated surface. This is shown in Figure 10B which shows the specific rate constant at 333 K as a function of the development of the catalyst, calculated from the data in Figure 9B and C. It appears, therefore, that the efficacy of the catalyst in nitrate reduction once activated is a result of a morphology change which suppresses water reduction over nitrate reduction, rather than activating the nitrate reduction itself.

Steady state nitrate reduction current densities obtained at a series of potentials are shown for both an unactivated (2) and activated (1) catalyst in Figure 11. Between the steady state measurements, carried out at the indicated potential, the electrode is cycled five times through the potential range −1.02 to +0.1 V in order to maintain its activity and structure. There is a clear difference between the steady state activities of the two catalysts. As one may expect on the basis of the voltammetry (Figure 1), the onset for nitrate reduction is observed at ca. −0.8 V, and increases for more negative potentials. The influence of the poisoning reaction on the steady state currents for the two catalysts is clearly evident. In the case of the unactivated electrode (2), at potentials in the range −0.8 to −0.95 V, the initial reduction current is higher. However, over the period of the steady state reaction (180 s) a strong decay of the current is evident as a result of the poisoning reaction. At more negative potentials this decay brings the steady state current below that of the activated electrode, and in fact the residual current observed at potentials below −1.0 V is a result of water reduction. The activated electrode (1) exhibits a lower initial reduction rate in the range −0.8 to −0.95 V, however only a very slow decay in the current is observed over the measured time interval of 180 s. At −1.0 to −1.1 V, steady state nitrate reduction currents still exhibit only a

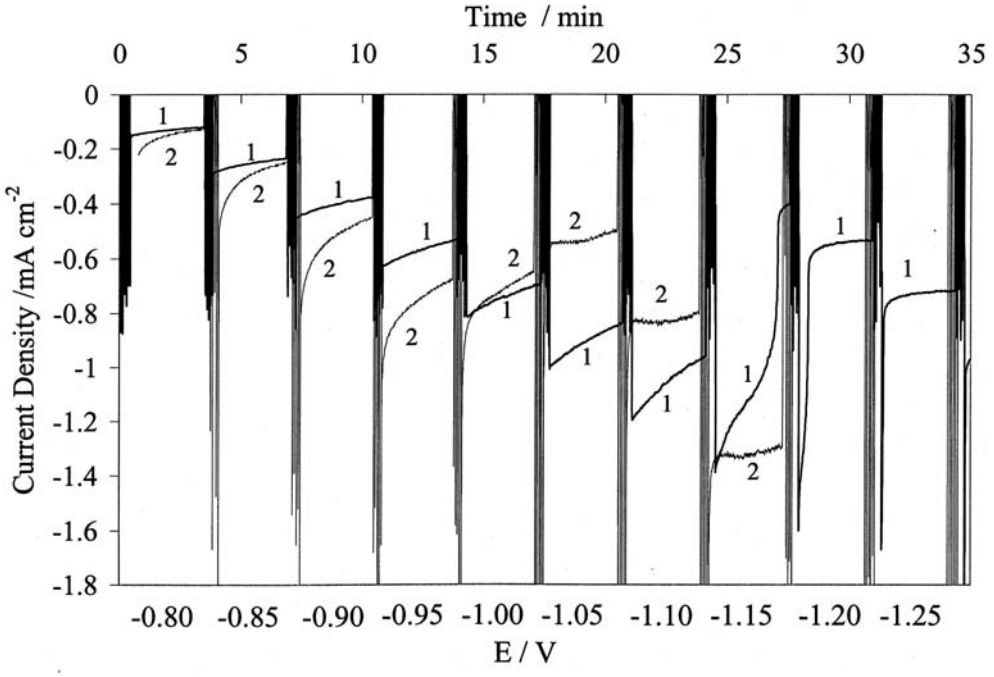

Fig. 11. Steady state nitrate reduction current densities at various potentials for the unactivated (1), and activated (2) catalyst. Between the steady state reduction current measurements the electrode was cycled five times (−1.025 to +0.1 V at 500 mV s^{-1}).

slow decay with time. The onset of poisoning associated with the water reduction reaction on the activated catalyst takes place in the steady state measurements at −1.15 and −1.20 V, where a sudden drop in the reduction current is observed during the steady state reaction. Only at even more negative potentials does water reduction dominate the steady state current on activated electrodes but even so the water reduction current is at a lower value than that for the unactivated surface at equivalent voltages (the water reduction current is off scale in Figure 11 for the unactivated surface at potentials below −1.15 V).

The slow decay of the reduction current on the activated electrode at more negative potentials also corresponds to higher steady state rates of nitrate reduction. One possible explanation for the slow degradation is the accumulation of adsorbed oxygen containing intermediates. However, at these potentials, their surface lifetime is expected to be very low. A more likely possibility is that their presence on the surface even as short lived intermediates may result in restructuring of the rhodium surface. However, a key observation in this regard is that steady state reduction in low concentrations of nitrate results in a faster deactivation of the catalyst. It is also observed that taking the potential to a more negative excursion during activation, into the water reduction region, also leads to catalyst deactivation (see above). It appears that the presence of nitrate, and hence the adsorbed oxygen containing intermediates, are both important in the activation process itself. We therefore suggest that it is the strongly reducing environment during hydrogen evolution, and the presence of the hydrogen intermediate, that leads to the direct fast poisoning of the reaction, which can also result in a slow deactivation through surface reconstruction.

3.3 *The structure of activated rhodium electrodes*

Figure 12 shows scanning electron micrographs obtained from rhodium electrode surfaces before and after activation. The imaged electrode is a 1 μm rhodium plated titanium surface. There is clearly a change in the form of the rhodium that takes place during activation. Figure 12A is an image of the unactivated surface (AF = 60), and exhibits a form expected from electroplating, i.e. a rough cracked surface showing evidence of a 'leafy' structure. Figure 12B shows that activation of the electrode (AF = 190) results in the formation of a 'sponge' like structure of diffuse spheres with diameters in the range 10–20 μm. The pores and particles in the sponge like structure cannot be resolved by SEM, but preliminary TEM images indicate rhodium particle sizes in the range 5–10 nm. This corresponds well with the electrochemical measurements that reveal effective AFs of the order of 230 times the geometric area of the electrode for the 1μm thick rhodinised electrodes. This corresponds to a catalyst area of ca. 19 $m^2 g^{-1}$, similar to areas found for platinum and rhodium blacks with particle sizes of ca. 7–10 nm.

4. Conclusions

The specific activity of electro-deposited rhodium films supported on titanium substrates towards nitrate

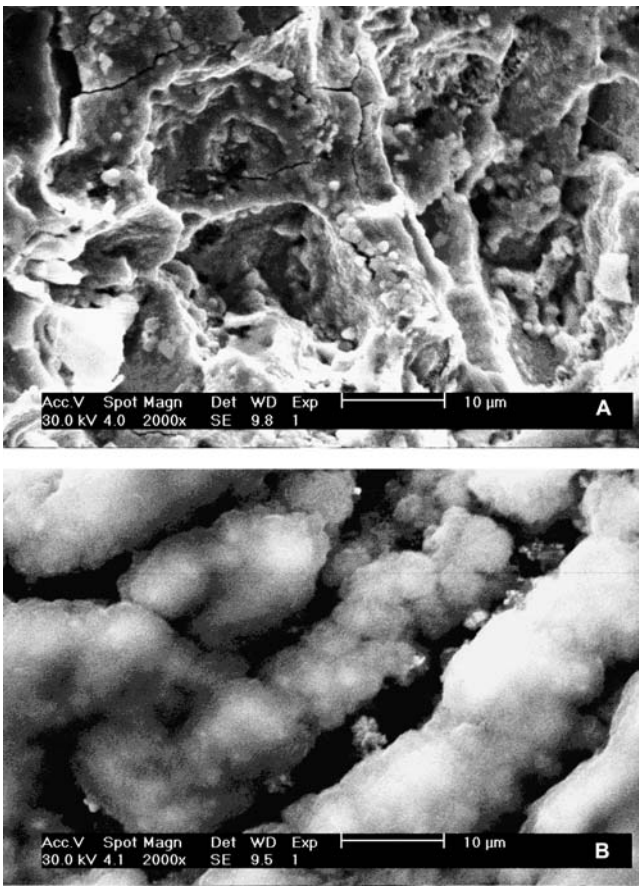

Fig. 12. Electron micrographs of the (A) unactivated (B) activated surfaces.

reduction has been investigated. At the overpotentials for reduction investigated, nitrate electro-reduction to N_2 takes place. A process that increases the surface area of the rhodium electrodes, and produces a surface with a high activity for nitrate reduction, has been developed. The activation process involves oxidation/reduction cycles in an alkaline, KCl electrolyte containing nitrate ions. Surfaces of up to 230 times the geometric area are achieved, together with a surface morphological modification. While the active surface, once formed, is intrinsically unstable during long-term nitrate reduction, its activity can be maintained *in situ* by a simple electrochemical cycling procedure.

The high area rhodium has the form of a nano-structured 'sponge', with a surface to weight ration of ca. $19\,m^2\,g^{-1}$. The morphological modification is evidenced by a change in the hydrogen UPD structure, an enhancement in OH adsorption and surface oxidation, and a reduction in the activation energy for nitrate reduction from 47 to $20\,kJ\,mol^{-1}$. The reduction in activation energy, however, is accompanied by a decrease in the pre-exponential factor, and this apparent compensation effect results in similar rate constants on the activated and unactivated surfaces. Surface morphology change does not significantly change the specific adsorption characteristics of the nitrate. The change in activation energy and the reduction in pre-exponential is tentatively ascribed to the formation of a relatively small number of sites which adsorb the reduction product (probably OH) more strongly resulting in a concomitant reduction in the activation barrier. The net enhancement in the catalytic activity for nitrate reduction results from an increase in the relative activity of nitrate reduction over water reduction. The activated catalyst sustains steady state nitrate reduction at an increased overpotential before the reaction to N_2 decays, and hydrogen evolution and reduction to ammonia take place.

The presence of nitrate ions is essential for the formation of the active surface, and specifically adsorbed nitrate ions and reductive intermediates are present at the surface when it is reformed. A mechanism for the elementary surface reaction steps involved in nitrate reduction, and the apparent 'habit' growth of the active surface phase in the nitrate containing solution is discussed.

Acknowledgements

Ionex Ltd acknowledges the financial support of the Environment Agency, Yorkshire Water plc and Johnson Matthey plc, without which this work could not have been undertaken.

References

1. L.W. Canter, 'Nitrates in Groundwater' (CRC Press, Boca Raton, FL, USA, 1996).
2. WHO, 'Guidelines for Drinking Water Quality', Vol. 2 (and Addendum) (World Health Organisation, 1996, 1998).
3. A. Kapoor and T. Viraraghavan, *J. Environ. Eng.* **123** (1997) 371.
4. V. Mateju, S. Cizinska, J. Krejei and T. Janoch, *Enzyme Microbiol. Technol.* **14** (1992) 170.
5. S. Horold, T. Tacke and K.D. Vorlop, *Environ. Technol.* **14** (1993) 931.
6. S. Horold, K.D. Vorlop, T. Tacke and M. Sell, *Catal. Today* **17** (1993) 21.
7. Y. Yoshinaga, T. Akita, I. Mikami and T. Okuhara, *J. Catal.* **207** (2002) 37.
8. G. Strukul, R. Gavagnin, F. Pinna, E. Modaferri, S. Perathoner, G. Centi, M. Marella and M. Tomaselli, *Catal. Today* **55** (2000) 139.
9. U. Prusse, M. Hahnlein, J. Daum and K.D. Vorlop, *Catal. Today* **55** (2000) 79.
10. A. Pintar, *Catal. Today* **77** (2003) 451.
11. A. Pintar, J. Batista and J. Levec, *Chem. Eng. Sci.* **56** (2001) 1551.
12. A. Pintar, J. Batista and J. Levec, *Catal. Today* **66** (2001) 503.
13. L. Lemaignen, C. Tong, V. Begon, R. Burch and D. Chadwick, *Catal. Today* **75** (2002) 43.
14. O.M. Ilinitch, F.P. Cuperus, L.V. Nosova and E.N. Gribov, *Catal. Today* **56** (2000) 137.
15. F. Epron, F. Gauthard and J. Barbier, *J. Catal.* **206** (2002) 363.
16. F. Epron, F. Gauthard and J. Barbier, *Appl. Catal. A – Gen.* **237** (2002) 253.
17. F. Deganello, L.F. Liotta, A. Macaluso, A.M. Venezia and G. Deganello, *Appl. Catal. B – Environ.* **24** (2000) 265.
18. J. Daum and K.D. Vorlop, *Chem. Ing. Tech.* **70** (1998) 1567.
19. K. Daub, V.K. Wunder and R. Dittmeyer, *Catal. Today* **67** (2001) 257.

20. D.H. Cloleman, R.E. White and D.T. Hobbs, *J. Electrochem. Soc.* **142** (1995) 1152.
21. E.E. Kalu, R.E. White and D.T. Hobbs, *J. Electrochem. Soc.* **143** (1996) 3094.
22. H. Li, J.Q. Chambers and D.T. Hobbs, *J. Appl. Electrochem.* **18** (1988) 454.
23. H. Li, D.H. Robertson, J.Q. Chambers and D.T. Hobbs, *J. Electrochem. Soc.* **135** (1988) 1154.
24. H.L. Lin, J.Q. Chambers and D.T. Hobbs, *J. Electroalal.Chem.* **256** (1988) 447.
25. J.D. Genders, D. Hartsough and D.T. Hobbs, *J. Appl. Electrochem.* **26** (1996) 1.
26. J.O.M. Bockris and J. Kim, *J. Appl. Electrochem.* **27** (1997) 623.
27. M. Waite, Water purification process, Patent GB 2348209; (Ionex Ltd., United Kingdom, 1998).
28. M. Waite, P.M. Tucker and B.E. Hayden, A processs for improving an electrode, Patent GB 2 365 023 B (Ionex Ltd., United Kingdom, 2000).
29. W. Plieth, in A.J. Bard (Ed), 'Encyclopedia of Electrochemistry of the Elements', Vol. 4, (Marcel Decker, New York, 1973).
30. M. Tokuoka, *Collect. Czech. Chem. Commun.* **4** (1932) 444.
31. G. Horanyi and E.M. Rizmayer, *J. Electroanal. Chem.* **188** (1985) 265.
32. O.A. Petrii and T.Y. Safonova, *J. Electroanal. Chem.* **331** (1992) 897.
33. M. da Cunha, J.P.I. De Souza and F.C. Nart, *Langmuir* **16** (2000) 771.
34. A.C. Chialvo, W.E. Triaca and A.J. Arvia, *J. Electroanal. Chem.* **237** (1987) 237.
35. R. Woods, *in* A.J. Bard (Ed), 'Electroanalytical Chemistry', Vol. 9 (Marcel Dekker, New York, 1976) p. 90.
36. M. Wasberg and G. Horanyi, *Electrochim. Acta* **40** (1995) 615.
37. C. Pallotta, N.R.D. Tacconi and A.J. Arvia, *J. Electroanal. Chem.* **159** (1983) 201.
38. E. Custidiano, S. Piovano, A.J. Arvia, A.C. Chialvo and M. Ipohorski, *J. Electroanal. Chem.* **221** (1987) 229.
39. I. Kostov and R.I. Kostov, 'Crystal Habits of Minerals' (Academic Publishing House and Pensoft, Sofia, 1999).
40. R.J. Davey, *in* E.J. de Jong and S.J. Jancic (Eds), 'Industrial Crystallization (7th Symposium, Warsaw)', (North Holland, Amsterdam, 1979) p. 169.
41. J. Prywer and S. Krukowski, *MRS Internet J. Nitride Semicond. Res.* **3** (1998) 47.
42. J. Prywer, *J. Crys. Growth* **158** (1996) 568.
43. B.A. Averill, I.M.C.M. Rietjens, P.W.N.M. van Leeuwen and R.A. van Santen, in R.A. van Santen, P.W.N.M. van Leeuwen, J.A. Moulijn and B.A. Averill (Eds), 'Catalysis: An Integrated Approach', (Elsevier Science, Amsterdam, 1999).
44. A.K. Galwey, *Adv. in Catal.* **26** (1977) 247.
45. G.C. Bond, A.D. Hooper, J.C. Slaa and A.O. Taylor, *J. Catal.* **163** (1996) 319.
46. G.C. Bond and R.H. Cunningham, *J. Catal.* **166** (1997) 172.
47. G.C. Bond, *Appl. Catal.* **191** (2000) 23.